electronics

MDPI

Article

Research on the Modeling of Bending-Torsional Coupling and Vibration Characteristics of Planetary Roller Screw Mechanism

Linping Wu [1], Shangjun Ma [1,2,*], Pan Deng [3] and Qiangqiang Huang [3]

[1] Shaanxi Engineering Laboratory for Transmissions and Controls, Northwestern Polytechnical University, Xi'an 710072, China; wulinping@mail.nwpu.edu.cn
[2] Xi'an Ding Bai Precision Technology Co., Ltd., Xi'an 710000, China
[3] Shanghai Marine Equipment Research Institute, Shanghai 201108, China; climberhit@163.com (P.D.); huangqiangqiang@mail.nwpu.edu.cn (Q.H.)
* Correspondence: mashangjun@nwpu.edu.cn; Tel.: +86-134-6867-0092

Abstract: A general bending-torsional coupling dynamic model of the planetary roller screw mechanism is developed by the lumped mass method in this paper to analyze the vibration characteristics. Firstly, the components of the planetary roller screw mechanism are treated as lumped mass, and the meshing relationships are expressed by the spring element. Secondly, the natural vibration characteristics of the planetary roller screw mechanism are analyzed, and four vibration modes based on the bending-torsional coupling dynamic model are summarized: carrier mode, torsional mode, transverse mode and roller mode. This reveals the vibration characteristics when the two kinds of meshing pairs (thread pair and gear pair) come into meshing synchronously. Then, the relationships between the structural parameters and the natural frequency of each vibration mode are discussed. Finally, the matrix equation is simplified according to the characteristics of vibration mode, and the analytic expressions of natural frequency under carrier mode and roller mode are obtained.

Keywords: planetary roller screw mechanism; lumped mass method; bending-torsional coupling dynamic model; natural vibration characteristics; natural frequency

Citation: Wu, L.; Ma, S.; Deng, P.; Huang, Q. Research on the Modeling of Bending-Torsional Coupling and Vibration Characteristics of Planetary Roller Screw Mechanism. *Electronics* **2022**, *11*, 1395. https://doi.org/10.3390/electronics11091395

Academic Editor: Davide Astolfi

Received: 24 March 2022
Accepted: 24 April 2022
Published: 27 April 2022

1. Introduction

With the development of equipment automation and intelligence and the wide application of electromechanical actuator in industrial fields, electromechanical servo actuation system is developing in the direction of high power, high integration, high precision and high reliability. As an actuator that converts rotational motion into linear motion [1], the planetary roller screw mechanism (PRSM) has gradually become one of the best choices of the electromechanical servo actuation system because of its high load capacity, long service life and convenient installation and maintenance. PRSM mainly transmits power and motion through point contact between threaded teeth. The motion relationship of the components in the standard PRSM is called forward transmission, that is, the screw rotates around its axis, and the nut, as the output component, moves back and forth along the axis. As shown in Figure 1, this is the structure of a standard PRSM, which is mainly composed of screw, nut, roller, ring gear and carrier. The specific structure is that the screw and the nut are processed as multi-starts; the thread on roller is manufactured as a single start. Rollers will participate in the meshing of two types of meshing pairs (thread pair and gear pair) at the same time and are evenly distributed around the screw by the carrier, and the motion is transmitted to the nut through the "planetary motion" of the roller. The carrier does not participate in any meshing motion, and its moving position is controlled by the spring retainer.

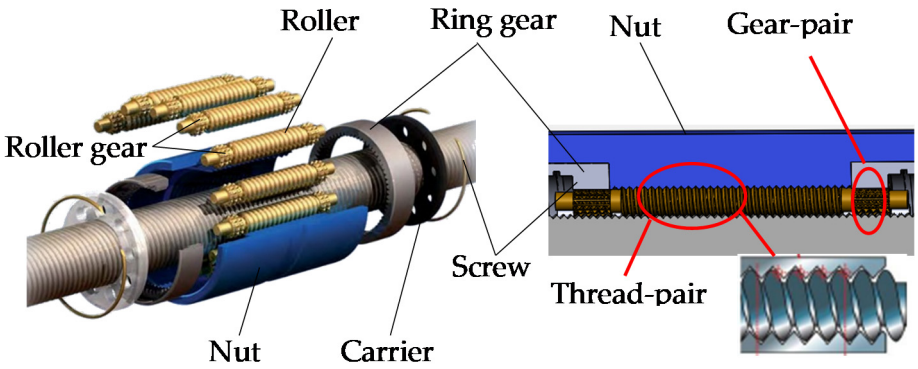

Figure 1. Structure of the standard PRSM.

The unique structural composition and transmission form of PRSM make its static stiffness about 50% higher than that of a ball screw under the same diameter. When bearing the same axial load, its installation space is saved by 1/3 times, and its working life is increased by about 14 times [2]. The transmission accuracy of a PRSM system can also be improved by adopting the micro-lead design. These advantages can effectively solve the bottleneck problem of realizing a more stable and ultra-high precision transmission under light load and heavy load conditions in a limited installation space. Presently, electromechanical servo technology based on PRSM has been adopted in the fields of aircraft rudder, high–low drive of tank, continuous variable transmission, feed of high-grade numerical control machines, swing arm of a welding robot and other fully electromechanical equipment at home and abroad [3–7].

The important points found in the research are that the meshing contact state of PRSM determines the transmission performance of the mechanism, and its dynamic response characteristics reflect the quality of the contact state of the system. In recent years, the research on PRSM has mainly focused on contact characteristics, load distribution, kinematic analysis and dynamics.

The contact state of PRSM refers to the deformation of thread teeth under load and the position of the contact point. Liu et al. analyzed the theoretical position of the contact point based on the helical surface equation and the meshing equation between two threaded surfaces and compared the change of the contact position when the roller is in a different tooth profile [8,9]. Based on the study of thread contact characteristics, Ma et al. optimized the meshing clearance by optimizing structural parameters and calculated the size and principal curvature direction of the contact ellipse at the contact point according to the principle of differential geometry. Moreover, the contact characteristics of the contact surface between the screw and the roller or between the roller and the nut under the joint action of normal pressure and tangential friction are analyzed, and two different contact states are obtained [10–12]. Hojjat et al. revealed the influence law of the roller thread direction on the rolling and sliding phenomenon in the motion through the analysis of the stress state of the roller and verified it with experiments [13]. Jones et al. established the analytical meshing model of PRSM by using the tangent contact condition of the curved surface and calculated the contact positions between the screw-roller and nut-roller interfaces. Then, the load-bearing thread is discretized into spring group, and the load distribution is proposed by the direct stiffness method [14,15]. Sandu et al. deduced the thread surface equation when the thread section of the component in PRSM is plane, convex and concave, and calculated the meshing point position between the contact threads considering the axial clearance. Further, the geometric shape and size of the contact ellipse on the screw side were obtained by solving the generalized equations. On this basis, an analytical model for solving the sliding velocity at any point in the contact area was established and compared with the experimental results [16,17].

In addition, the research results of Vahid et al. show that thread pair errors and friction are the main factors leading to vibration [18]. Jones et al. discussed the relationship between

the relative sliding distance and the lead considering the axial deflection of the roller. Jones et al. established the rigid body dynamic model of PRSM and calculated the angular velocity, angular acceleration and rolling sliding velocity at the contact point, respectively. The model mentioned can accurately simulate the motion state of PRSM through steady-state and transient kinematic analysis [19,20]. Abevi et al. described the load distribution model by taking the interaction between the thread tooth as beam, the rod and the nonlinear spring element, and conducted an experimental study on the load distribution state between the rollers [21,22]. Ma et al. set up a bond graph dynamic model considering the clearance, friction, deformation and error, focusing on the influence of PRSM friction characteristics on dynamic performance [23]. Guo et al. proposed the dynamic modeling method of PRSM when considering the thread contact stiffness, analyzing the influence of the change of contact angle under different roller radii and the change of roller radius under different contact angle on the contact stiffness [24]. Wu et al. suggested that the lumped mass method can be used to establish the pure torsional model of PRSM. Based on the dynamic differential equations, the relationship between the natural frequency and the number of rollers is discussed, and it is concluded that there are two typical vibration modes of the PRSM [25]. After researching the dynamic behavior of PRSM under light load and heavy load, Fu et al. pointed out that the error is the main reason for the difference of contact state and the uncoordinated motion of multiple rollers [26,27]. By using equivalent load and deformation to equivalent axial load, Du et al. established a mechanical model considering the machining error and radial force. Meanwhile, machining errors were shown to increase the unevenness of the load distribution and consequently reduce the lifespan of PRSM [28]. Based on the influence law of the machining error on lifespan proposed in Ref. [28], Lepagneul et al. proposed a fatigue life design strategy suitable for standard and inverted PRSM according to the Hertz contact model. Additionally, the loading range of infinite life of the mechanism is deduced by using the Dang van criterion [29]. The models mentioned above on meshing characteristics, kinematics and dynamics were simplified, and there is a lack of generality of the model, which cannot reveal the motion characteristics of the two types of meshing pairs during synchronous meshing, nor reflect the relationship between the meshing pairs and the vibration characteristics of the PRSM.

In order to improve the dynamic transmission performance of PRSM, this paper mainly carries out the dynamic modeling when two pairs are in contact at the same time and the analysis of vibration characteristics. This paper proposes a general bending-torsional coupling dynamic model of PRSM by using the lumped mass method. In the model, each component is regarded as a lumped mass, and the spring element is used to represent the meshing relationship between components. The whole PRSM transmission system is regarded as a spring-mass system. First, according to the derivation of relative displacement between components, the dynamic differential equations of the system are derived based on Newton's second law. Second, the stiffness parameters, such as thread contact stiffness, meshing stiffness, bending stiffness and torsional stiffness, are introduced, which are calculated by the analytical method and finite element method. Then, the natural vibration characteristics of the PRSM are analyzed, and four vibration forms according to the bending-torsional coupling dynamic model are summarized: carrier mode, torsional mode, transverse mode and roller mode. Finally, the correctness of the bending-torsional coupling dynamic model proposed is verified from three aspects. This provides guidance for improving the comprehensive dynamic performance of PRSM.

2. Bending-Torsional Coupling Dynamic Model

2.1. Modeling

In this paper, two different coordinate systems are used for modeling. One is the overall coordinate system of PRSM, which is also the fixed coordinate system of the screw, ring gear, nut and carrier. The other group is the local rotating coordinate system of the roller, which is convenient to describe the roller position with a constant angle value. As shown in Figure 2, the coordinate origin of the coordinate system *o-xyz* is fixed on the axis

of the screw, which does not rotate with the rotation of the carrier, and the x direction points to the static balance position of the first roller. The coordinate origin of the local rotating coordinate system o_{Ri}-$x_{Ri}y_{Ri}z_{Ri}$ (i = 1, 2, . . . , N) is located on the axis of the i-th roller and rotates at a constant speed with the carrier, so as to ensure that the z_{Ri} axis always points to the axis direction of roller i and coincides with its rotation. Meanwhile, the dynamic model of the rollers is established in the local rotating coordinate system.

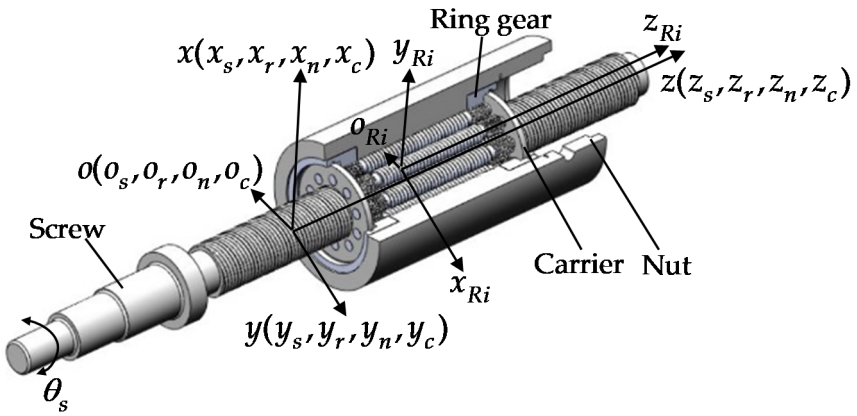

Figure 2. The coordinate system of standard PRSM.

The following assumptions are adopted in the modeling: (1) The multi-point contact between the thread pairs in the PRSM is regarded as line contact; (2) The meshing relationship between threads is simplified as a spring element in the tangential direction at the contact point [21,22], and the stiffness of the spring is the contact stiffness of the thread; (3) It is considered that the mass and moment of the inertia of each roller are equal, and they are evenly distributed around the screw; (4) The thread contact stiffness of each roller with the screw and nut, as well as the meshing stiffness with the ring gear, are equal, respectively, and there is only a phase difference; (5) The bending stiffness of the screw, nut and ring gear in x and y directions is equal.

The bending-torsional coupling dynamic model of PRSM shown in Figure 3 θ_j (j = s, r, n, Ri, c) is the angular displacement of screw, ring gear, nut, roller and carrier due to system vibration. Components with such degrees of freedom include the screw, carrier, ring gear, nut and N rollers, and the number of torsional degrees of freedom is n + 4; x_j, y_j is the displacement of the center of mass of the components along the x and y directions, and there are six translational degrees of freedom. Therefore, the lumped mass dynamic model of PRSM in this paper contains a total of (n + 10) degrees of freedom. The meshing relationship between the screw and the roller is described by the spring element K_{sR}. Similarly, the spring elements K_{rR} and K_{nR} are used to represent the meshing relationship between the roller and the ring gear, as well as between the roller and the nut, respectively; Ksx and Ksy is the bending stiffness of the screw in two directions, as shown in Table 1.

Table 1. The definition of parameters.

Symbol	Description
θ_j (j = s, r, n, Ri, c)	Angular displacement of screw, ring gear, nut, roller, carrier
n + 4	The number of torsional degrees of freedom
6	The number of translational degrees of freedom
K_{sR}	Thread meshing stiffness between screw and roller
K_{rR}	Spur gear meshing stiffness between ring gear and roller
K_{nR}	Thread meshing stiffness between nut and roller
Ksx	Bending stiffness of the screw in x direction
Ksy	Bending stiffness of the screw in y direction

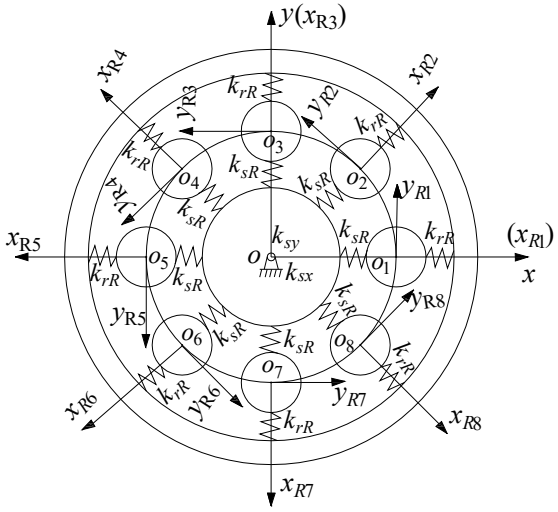

Figure 3. Bending-torsional coupling model of PRSM.

2.2. Relative Displacement

According to assumptions (1) and (2), in order to facilitate the derivation of relative displacement, Equations (1)–(5) can be used to convert the torsional angle displacement of screw, ring gear, nut, roller and carrier into tangential line displacement around their respective axis of contact point position.

$$u_s = r_{s0} \cdot \theta_s \tag{1}$$

$$u_r = r_{r0} \cdot \theta_r \tag{2}$$

$$u_n = r_{n0} \cdot \theta_n \tag{3}$$

$$u_{Ri} = r_{R0} \cdot \theta_{Ri} \tag{4}$$

$$u_c = r_{c0} \cdot \theta_c \tag{5}$$

where r_{s0}, r_{n0} and r_{R0} are the nominal radii of the screw, nut and roller, respectively; r_{r0} is the pitch circle radius of the ring gear; r_{c0} is the nominal radius of the carrier, which can be expressed by

$$r_{c0} = r_{s0} + r_{R0} \tag{6}$$

When the PRSM is loaded, the contact force between the thread teeth follows the normal direction of its spatial helical surface, which can be divided into three directions. The forces state of thread pairs as shown in Figure 4: F_{xa} is the axial force, F_{xt} is the tangential force of the normal load, and F_{xr} is the radial force. β_s is the helix angle of the screw, β_n is the helix angle of the nut, α_{sc} is the normal contact angle between the screw and the roller, α_{nc} is the normal contact angle between the screw and the roller.

2.2.1. Roller-Screw

As shown in Figure 5, the contact position relationship between the screw and the roller is shown. The relative displacement between the screw and the roller can be obtained by projecting the vibration displacement of the screw and the roller to the tangent direction of the contact point on the roller–screw contact side. The projection of the line displacement x_s and y_s of the center of mass of the screw to the tangent direction of the contact point is $-x_s \cdot \sin\phi_{si}$ and $-y_s \cdot \cos\phi_{si}$. Its torsional linear displacement is u_s. Similarly, the torsional linear displacement of the roller is $u_{Ri.}$ Therefore, the projection of the relative displacement on the roller–screw contact side can be written as

$$\delta_{sRi} = (y_s \cos\phi_{si} - x_s \sin\phi_{si} + u_s + u_{Ri}) \cos\beta_s \tag{7}$$

$$\phi_{si} = \alpha_{sc} - \phi_i \tag{8}$$

where α_{sc} is the contact angle on the roller–screw contact side; β_s is the helix angle of the screw; ϕ_i is the included angle between the connecting line, which consists of the axis of the i-th roller and the coordinate origin, and the positive direction of the x. It is also the phase angle of the i-th roller, which can be expressed as

$$\phi_i = 2\pi(i-1)/N \tag{9}$$

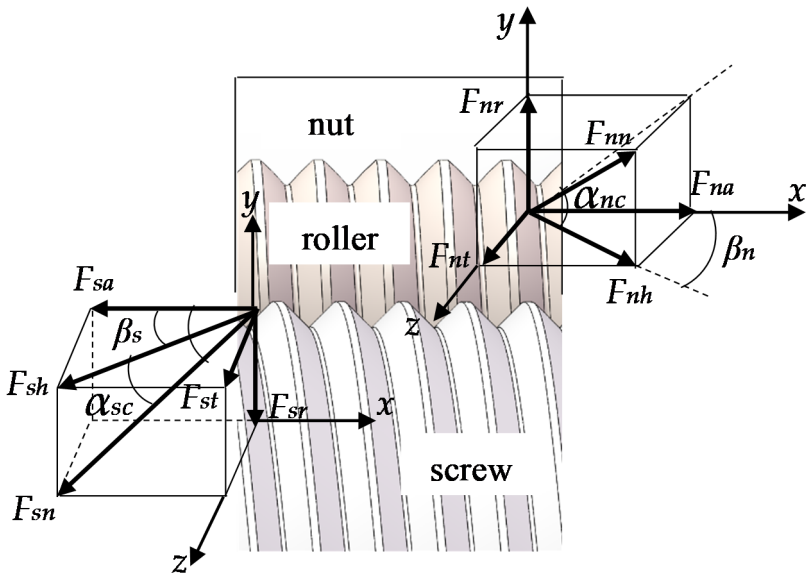

Figure 4. The forces state of thread pairs.

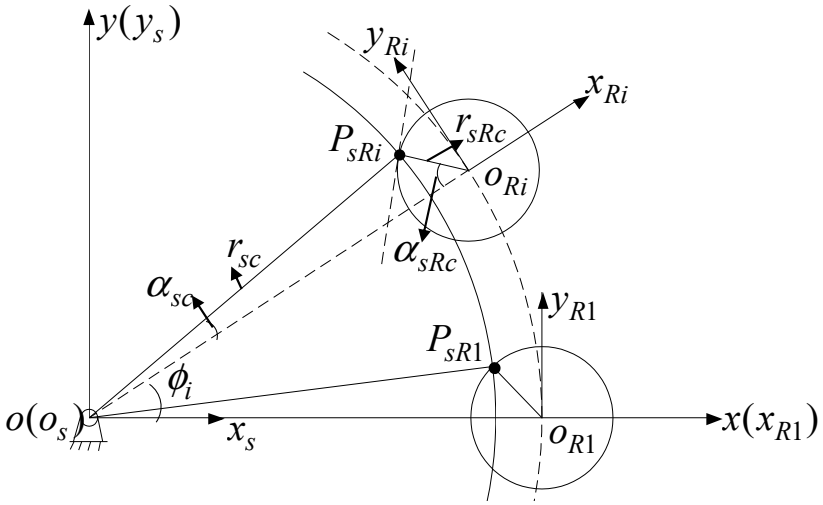

Figure 5. Contact position between the screw and the i-th roller.

2.2.2. Roller-Ring Gear

The relative position relationship between the ring gear and the i-th roller in the meshing state is shown in Figure 6. It is assumed that the displacement is positive when the spring produces compression deformation, which is equivalent to the meshing relationship between the ring gear and the roller. $-x_r \cdot \sin\phi_{ri}$ and $y_r \cdot \cos\phi_{ri}$, respectively, represent the projection of the line displacement of the center of mass of the ring gear along the line of

action. $-u_{Ri}$ is the projection of the torsional line displacement of the roller. The relative vibration displacement projection can be expressed by

$$\delta_{rRi} = y_r \cos\phi_{ri} - x_r \sin\phi_{ri} + u_r - u_{Ri} \tag{10}$$

$$\phi_{ri} = \alpha_r + \phi_i \tag{11}$$

where α_r is the contact angle of the ring gear.

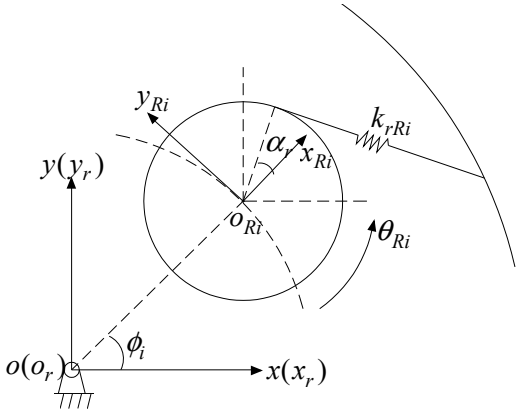

Figure 6. Contact position between the ring gear and the *i*-th roller.

2.2.3. Roller-Nut

Figure 7 shows the contact position relationship between the roller and the nut. The relative displacement can be obtained by projecting the displacement between the roller and the nut to the tangent direction of the contact point. The projection of the transverse line displacement x_n and y_n of the center of mass of the nut is $-x_n \cdot \sin\phi_{ni}$ and $y_n \cdot \cos\phi_{ni}$, respectively, and its torsional line displacement is u_n. The relative displacement δ_{nRi} on the roller–nut contact side can be described as

$$\delta_{nRi} = (y_n \cos\phi_{ni} - x_n \sin\phi_{ni} + u_n - u_{Ri}) \cos\beta_n \tag{12}$$

$$\phi_{ni} = \alpha_{nc} + \phi_i \tag{13}$$

where α_{nc} is the contact angle on the roller–nut contact side. β_n is the helix angle of the nut.

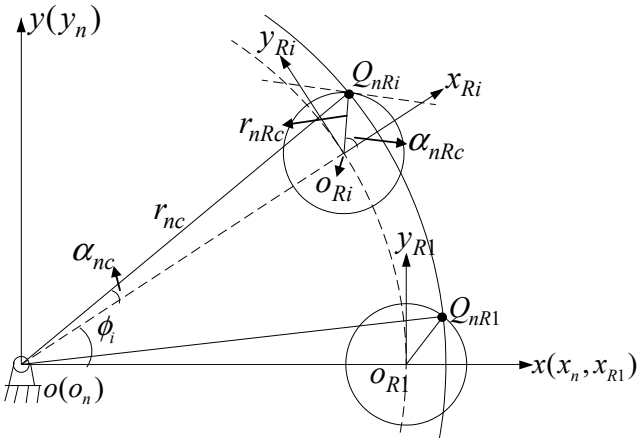

Figure 7. Contact position between the nut and the *i*-th roller.

2.3. Dynamic Differential Equations

It can be seen from Figure 4 that t the x direction is the direction of axial force, and the y axis coincides with the radial force direction. Additionally, the projection relationship

between the contact force and any of the other three directional forces can also be obtained. According to the motion principle of the PRSM and the bending-torsional coupling dynamic model proposed in this paper, the dynamic differential equations of each main component, which includes the screw, ring gear, nut, roller and carrier, can be deduced based on Newton's second law.

$$\begin{cases} m_s\ddot{x}_s + K_{sx}x_s + \sum\limits_{i=1}^{N} K_{sRi}(y_s\cos\phi_{si} - x_s\sin\phi_{si} + u_s + u_{Ri})\cos\beta_s\sin\phi_{si}\cos\beta_s = 0 \\ m_s\ddot{y}_s + K_{sy}y_s - \sum\limits_{i=1}^{N} K_{sRi}(y_s\cos\phi_{si} - x_s\sin\phi_{si} + u_s + u_{Ri})\cos\beta_s\cos\phi_{si}\cos\beta_s = 0 \\ m_{eq,s}\ddot{u}_s + K_{su}u_s - \sum\limits_{i=1}^{N} K_{sRi}(y_s\cos\phi_{si} - x_s\sin\phi_{si} + u_s + u_{Ri})\cos\beta_s\cos\beta_s = 0 \end{cases} \tag{14}$$

$$\begin{cases} m_r\ddot{x}_r + K_{rx}x_r + \sum\limits_{i=1}^{N} K_{rRi}(y_r\cos\phi_{ri} - x_r\sin\phi_{ri} + u_r - u_{Ri})\sin\phi_{ri} = 0 \\ m_r\ddot{y}_r + K_{ry}y_r - \sum\limits_{i=1}^{N} K_{rRi}(y_r\cos\phi_{ri} - x_r\sin\phi_{ri} + u_r - u_{Ri})\cos\phi_{ri} = 0 \\ m_{eq,r}\ddot{u}_r + K_{ru}u_r - \sum\limits_{i=1}^{N} K_{rRi}(y_r\cos\phi_{ri} - x_r\sin\phi_{ri} + u_r - u_{Ri}) = 0 \end{cases} \tag{15}$$

$$\begin{cases} m_n\ddot{x}_n + K_{nx}x_n + \sum\limits_{i=1}^{N} K_{nRi}(y_n\cos\phi_{ni} - x_n\sin\phi_{ni} + u_n - u_{Ri})\cos\beta_n\sin\phi_{ni}\cos\beta_n = 0 \\ m_n\ddot{y}_n + K_{ny}y_n - \sum\limits_{i=1}^{N} K_{nRi}(y_n\cos\phi_{ni} - x_n\sin\phi_{ni} + u_n - u_{Ri})\cos\beta_n\cos\phi_{ni}\cos\beta_n = 0 \\ m_{eq,n}\ddot{u}_n + K_{nu}u_n - \sum\limits_{i=1}^{N} K_{nRi}(y_n\cos\phi_{ni} - x_n\sin\phi_{ni} + u_n - u_{Ri})\cos\beta_n\cos\beta_n = 0 \end{cases} \tag{16}$$

$$\begin{cases} m_{eq,R1}\ddot{u}_{R1} - K_{sR1}(y_s\cos\phi_{s1} - x_s\sin\phi_{s1} + u_s + u_{R1})\cos\beta_s\cos\beta_s \\ -K_{rR1}(y_r\cos\phi_{r1} - x_r\sin\phi_{r1} + u_r - u_{R1}) \\ -K_{nR1}(y_n\cos\phi_{n1} - x_n\sin\phi_{n1} + u_n - u_{R1})\cos\beta_n\cos\beta_n = 0 \\ \vdots \\ m_{eq,Ri}\ddot{u}_{Ri} - K_{sRi}(y_s\cos\phi_{si} - x_s\sin\phi_{si} + u_s + u_{Ri})\cos\beta_s\cos\beta_s \\ -K_{rRi}(y_r\cos\phi_{ri} - x_r\sin\phi_{ri} + u_r - u_{Ri}) \\ -K_{nRi}(y_n\cos\phi_{ni} - x_n\sin\phi_{ni} + u_n - u_{Ri})\cos\beta_n\cos\beta_n = 0 \end{cases} \tag{17}$$

$$\frac{J_c + \sum\limits_{i=1}^{N} m_{Ri}r_c^2}{r_{c0}^2}\ddot{u}_c + K_{cu}u_c = 0 \tag{18}$$

where N is the number of rollers; m_s, m_r, m_n, m_{Ri} represent the mass of the screw, ring gear, nut and roller, and $m_{eq,s}$, $m_{eq,r}$, $m_{eq,n}$, $m_{eq,Ri}$ are their equivalent mass, respectively. K_{jq} (j = s, r, n, Ri, c) (q = x, y) (i = 1, 2, . . . , N) is the bending stiffness; K_{ju} is the torsional stiffness; K_{jRi} is the meshing stiffness between the component and the i-th roller; u_j (j = s, r, n, Ri, c) is the tangential displacement; J_c and r_c are the moment of inertia and nominal radius of the carrier.

The matrix form of the dynamic differential equations can be written as

$$\boldsymbol{M}\cdot\ddot{\boldsymbol{\delta}} + (\boldsymbol{K}_b + \boldsymbol{K}_m)\cdot\boldsymbol{\delta} = 0 \tag{19}$$

where $\boldsymbol{M}$ is the mass matrix; $\boldsymbol{\delta}$ is the displacement matrix; $\boldsymbol{K}_b$ are $\boldsymbol{K}_m$ the support stiffness matrix and meshing stiffness matrix, respectively. The specific parameters of the $\boldsymbol{\delta}$, $\boldsymbol{M}$, $\boldsymbol{K}_b$ and $\boldsymbol{K}_m$ are shown in Equations (20)–(34).

$$\boldsymbol{\delta} = [x_s, y_s, u_s, x_r, y_r, u_r, x_n, y_n, u_n, u_{R1}, \cdots, u_{RN}, u_c]^{\mathrm{T}} \tag{20}$$

$$\boldsymbol{M} = diag\left[m_s, m_s, m_{eq,s}, m_r, m_r, m_{eq,r}, m_n, m_n, m_{eq,n}, m_{eq,R1}, \cdots, m_{eq,RN}, \frac{J_c + \sum_{i=1}^{N} m_{Ri} r_{c0}^2}{r_{c0}^2} \right] \tag{21}$$

$$\boldsymbol{K}_b = diag\left[K_{sx}, K_{sy}, K_{su}, K_{rx}, K_{ry}, K_{ru}, K_{nx}, K_{ny}, K_{nu}, 0, \cdots, 0, K_{cu} \right] \tag{22}$$

$$\boldsymbol{K}_m = \begin{bmatrix} \boldsymbol{k}_s & \boldsymbol{k}_0 & \boldsymbol{k}_0 & \boldsymbol{k}_{s1} & \cdots & \boldsymbol{k}_{sN} & \boldsymbol{o}_1 \\ & \boldsymbol{k}_r & \boldsymbol{k}_0 & \boldsymbol{k}_{r1} & \cdots & \boldsymbol{k}_{rN} & \boldsymbol{o}_1 \\ & & \boldsymbol{k}_n & \boldsymbol{k}_{n1} & \cdots & \boldsymbol{k}_{nN} & \boldsymbol{o}_1 \\ & & & k_{R1} & \cdots & 0 & 0 \\ & & & & \ddots & \vdots & \vdots \\ & & symmetric & & & k_{RN} & 0 \\ & & & & & & 0 \end{bmatrix} \tag{23}$$

where

$$\boldsymbol{k}_s = \begin{bmatrix} -\sum_{i=1}^{N} K_{sRi} \sin^2\phi_{si} \cos^2\beta_R & \sum_{i=1}^{N} K_{sRi} \cos\phi_{si} \sin\phi_{si} \cos^2\beta_R & \sum_{i=1}^{N} K_{sRi} \sin\phi_{si} \cos^2\beta_R \\ & -\sum_{i=1}^{N} K_{sRi} \cos^2\phi_{si} \cos^2\beta_R & -\sum_{i=1}^{N} K_{sRi} \cos\phi_{si} \cos^2\beta_R \\ symmetric & & -\sum_{i=1}^{N} K_{sRi} \cos^2\beta_R \end{bmatrix} \tag{24}$$

$$\boldsymbol{k}_r = \begin{bmatrix} -\sum_{i=1}^{N} K_{rRi} \sin^2\phi_{ri} & \sum_{i=1}^{N} K_{rRi} \cos\phi_{ri} \sin\phi_{si} & \sum_{i=1}^{N} K_{rRi} \sin\phi_{ri} \\ & -\sum_{i=1}^{N} K_{rRi} \cos^2\phi_{si} & -\sum_{i=1}^{N} K_{rRi} \cos\phi_{ri} \\ symmetric & & -\sum_{i=1}^{N} K_{rRi} \end{bmatrix} \tag{25}$$

$$\boldsymbol{k}_n = \begin{bmatrix} -\sum_{i=1}^{N} K_{nRi} \sin^2\phi_{ni} \cos^2\beta_R & \sum_{i=1}^{N} K_{nRi} \cos\phi_{ni} \sin\phi_{ni} \cos^2\beta_R & \sum_{i=1}^{N} K_{nRi} \sin\phi_{ni} \cos^2\beta_R \\ & -\sum_{i=1}^{N} K_{nRi} \cos^2\phi_{ni} \cos^2\beta_R & -\sum_{i=1}^{N} K_{nRi} \cos\phi_{ni} \cos^2\beta_R \\ symmetric & & -\sum_{i=1}^{N} K_{nRi} \cos^2\beta_R \end{bmatrix} \tag{26}$$

$$\begin{cases} k_{R1} = k_{R1}(1) + k_{R1}(2) + k_{R1}(3) \\ \vdots \\ k_{RN} = k_{RN}(1) + k_{RN}(2) + k_{RN}(3) \end{cases} \tag{27}$$

$$\boldsymbol{k}_0 = \begin{bmatrix} 0 & 0 & 0 \\ 0 & 0 & 0 \\ 0 & 0 & 0 \end{bmatrix} \tag{28}$$

$$\boldsymbol{o}_1 = \begin{bmatrix} 0 \\ 0 \\ 0 \end{bmatrix} \tag{29}$$

$$\begin{cases} \boldsymbol{k}_{s1} = \begin{bmatrix} K_{sR1}\sin\phi_{s1}\cos^2\beta_R \\ -K_{sR1}\cos\phi_{s1}\cos^2\beta_R \\ -K_{sR1}\cos^2\beta_R \end{bmatrix} \\ \vdots \\ \boldsymbol{k}_{sN} = \begin{bmatrix} K_{sRN}\sin\phi_{sN}\cos^2\beta_R \\ -K_{sRN}\cos\phi_{sN}\cos^2\beta_R \\ -K_{sRN}\cos^2\beta_R \end{bmatrix} \end{cases} \tag{30}$$

$$\begin{cases} \boldsymbol{k}_{r1} = \begin{bmatrix} -K_{rR1}\sin\phi_{r1} \\ K_{rR1}\cos\phi_{r1} \\ K_{rR1} \end{bmatrix} \\ \vdots \\ \boldsymbol{k}_{rN} = \begin{bmatrix} -K_{rRN}\sin\phi_{rN} \\ K_{rRN}\cos\phi_{rN} \\ K_{rRN} \end{bmatrix} \end{cases} \tag{31}$$

$$\begin{cases} \boldsymbol{k}_{n1} = \begin{bmatrix} -K_{nR1}\sin\phi_{n1}\cos^2\beta_R \\ K_{nR1}\cos\phi_{n1}\cos^2\beta_R \\ K_{nR1}\cos^2\beta_R \end{bmatrix} \\ \vdots \\ \boldsymbol{k}_{nN} = \begin{bmatrix} -K_{nRN}\sin\phi_{nN}\cos^2\beta_R \\ K_{nRN}\cos\phi_{nN}\cos^2\beta_R \\ K_{nRN}\cos^2\beta_R \end{bmatrix} \end{cases} \tag{32}$$

$$k_{R1} = -K_{sR1}\cos^2\beta_R + K_{rR1} + K_{nR1}\cos^2\beta_R \tag{33}$$

$$k_{RN} = -K_{sRN}\cos^2\beta_R + K_{rRN} + K_{nRN}\cos^2\beta_R \tag{34}$$

2.4. Parameters

2.4.1. Mass

As the torsional angular displacement is converted to the linear displacement, it indicates that the equivalent mass can be calculated in Equation (35):

$$m_{eq,j} = \frac{J_j}{r_{j0}^2}(j = s, r, n, R_i)(i = 1, 2, \ldots, N) \tag{35}$$

where J_j is the moment of inertia of component j. For the ring gear, r_{j0} is the radius of pitch circle; for the screw, nut and roller, r_{j0} is the nominal radius.

2.4.2. Contact Stiffness of Thread

The working load of PRSM is mainly the axial load, which realizes the bearing and power transmission through thread surface contact. It is obvious that the deformation of the screw, roller and nut after bearing is the main factor affecting the stiffness of the thread. In this paper, it is assumed that the axial load of PRSM is evenly distributed among each thread, and the thread contact stiffness is defined as the ratio of the load at the contact point to the contact deformation. According to the Hertz contact theory, the normal contact deformation on the roller–screw contact side or the roller–nut side can be given by [30]

$$\delta_{jRn} = \frac{2K(e)}{\pi m_a} \cdot \left[\frac{3F_n E'}{2\sum\rho}\right]^{\frac{2}{3}} \cdot \frac{\sum\rho}{2}(j = s \text{ or } n) \tag{36}$$

where $K(e)$ is the first kind of elliptic integral, and e is the eccentricity; $\Sigma\rho$ is the sum of the principal curvatures of the contact component; F_n is the normal contact force; E' is the

equivalent elastic modulus, which can be expressed by Equations (37) and (38); m_a is the function of the principal curvature $F(\rho)$, which can be obtained by [31]

$$F_n = \frac{F_a}{\cos\beta_R \cdot \sin\lambda} \tag{37}$$

$$E' = \frac{1-\mu_R^2}{E_R} + \frac{1-\mu_j^2}{E_j} \tag{38}$$

$$F(\rho) = \frac{\left|(\rho_{jj} - \rho_{jR}) + (\rho_{Rj} - \rho_{RR})\right|}{\sum\rho} \tag{39}$$

where F_a is the axial contact force; β_R is the helical angle of the roller; λ is the flank angle of the thread; μ_R and E_R are the Poisson's ratio and elastic modulus of the roller; μ_j and E_j are the material parameters of the screw or nut, respectively.

The magnitude of the principal curvature on the roller–screw side and on the roller–nut side can be described as

$$\rho_{ss} = \frac{1}{R},\ \rho_{sR} = \frac{1}{R} \tag{40}$$

$$\rho_{Rs} = 0,\ \rho_{RR} = \frac{2\cos\lambda}{d_c - 2R\cos\lambda} \tag{41}$$

$$\rho_{nn} = \frac{1}{R},\ \rho_{nR} = \frac{1}{R} \tag{42}$$

$$\rho_{Rn} = 0,\ \rho_{RR} = \frac{-2\cos\lambda}{d_c + 2R\cos\lambda} \tag{43}$$

where λ is the flank angle of the thread; d_c is the nominal diameter of the carrier; R is the equivalent spherical radius, which can be written as

$$R = \frac{d_R}{2\sin\alpha} \tag{44}$$

where d_R is the nominal diameter of the roller; d_c is also the revolution diameter of the roller, which can be expressed as $d_c = d_s + d_R$.

The axial contact deformation can be expressed by

$$\delta_{jRa} = \delta_{jRn} \cdot \cos\beta_R \cdot \sin\lambda \tag{45}$$

where δ_{jRn} is the normal contact deformation; β_R is the helical angle of the roller; λ is the flank angle of the thread.

When the threads mesh with each other, the normal contact stiffness and axial contact stiffness can be calculated with respect to the load and the deformation.

$$K_{jRn} = \frac{F_n}{\cos\beta_R \cdot \sin\lambda \cdot \delta_{jRn}} \tag{46}$$

$$K_{jRa} = \frac{F_a}{\delta_{jRa}} \tag{47}$$

where F_a is the axial contact force; K_{jRn} and $K_{jR}a$ are normal contact stiffness and axial contact stiffness, respectively.

2.4.3. Meshing Stiffness

The dynamic model of PRSM proposed is a concentrated mass model, which does not consider the distribution of the load along the tooth width direction. Therefore, the

meshing stiffness in this paper refers to the meshing stiffness of the full tooth width. The stiffness of a pair of teeth can be given by [32]

$$K = K' C_M C_R C_B \cos\beta \tag{48}$$

where C_M is the correction factor, C_R is the structure factor; C_B is the profile coefficient. Generally, C_M = 0.8, C_R = 1, C_B = 1. β is the helical angle of gear; K' is the theoretical value of stiffness of a pair of teeth, which can be expressed as

$$K' = \frac{1}{q'} \tag{49}$$

$$\begin{aligned} q' = {} & 0.04723 + \tfrac{0.15551}{z_{n1}} + \tfrac{0.25791}{z_{n2}} - 0.00635x_1 - 0.11654\tfrac{x_1}{z_{n1}} \\ & \mp 0.00193x_2 \mp 0.24188\tfrac{x_2}{z_{n2}} + 0.00529x_1^2 + 0.00182x_2^2 \end{aligned} \tag{50}$$

where q' is the minimum value of gear flexibility, and its unit is (mm·μm)/N; z_{n1} and z_{n2} are the equivalent number of teeth of pinion and large gear; x_1 and x_2 are the normal modification coefficients of pinion and large gear, respectively.

2.4.4. Bending Stiffness and Torsional Stiffness

The bending deformation and torsional deformation of the screw, roller, ring gear and nut are calculated by Ansys. When calculating the deformation, the boundary condition of the force is to couple each node of the loading surface with the center node of the face. Radial load Fr = 4000 N and torque T = 84 N·m are, respectively, applied to the central node when necessary. The displacement boundary conditions were set to impose fixed constraints on one end of the component. The scale of the finite element model is shown in Table 2.

Table 2. The scale of the finite element model.

Name	Number of Nodes	Number of Finite Elements
Screw	129,243	714,408
Roller	8090	34,918
Nut	203,766	772,994
Ring gear	20,306	96,336
Carrier	5576	22,881

Due to the action of gravity or radial load Fr, the bending deformation will occur on the component that is placed horizontally, and the bending stiffness can be written as Ref [33]. The torsional stiffness of each component can be calculated by Equation (52).

$$K_{jx(jy)} = \frac{F_r}{\tan\lambda \cdot \Delta y} \tag{51}$$

$$K_{ju} = \frac{T \cdot r_j}{\Delta y} \tag{52}$$

where Fr is the radial load; λ is the flank angle; T is the torque; r_j is the nominal radius of the component.

The bending deformations of the screw, roller, ring gear and nut under radial load are shown in Figure 8a–d; Figure 9a–d shows the torsional deformation of the screw, carrier, ring gear and nut when subjected to torque.

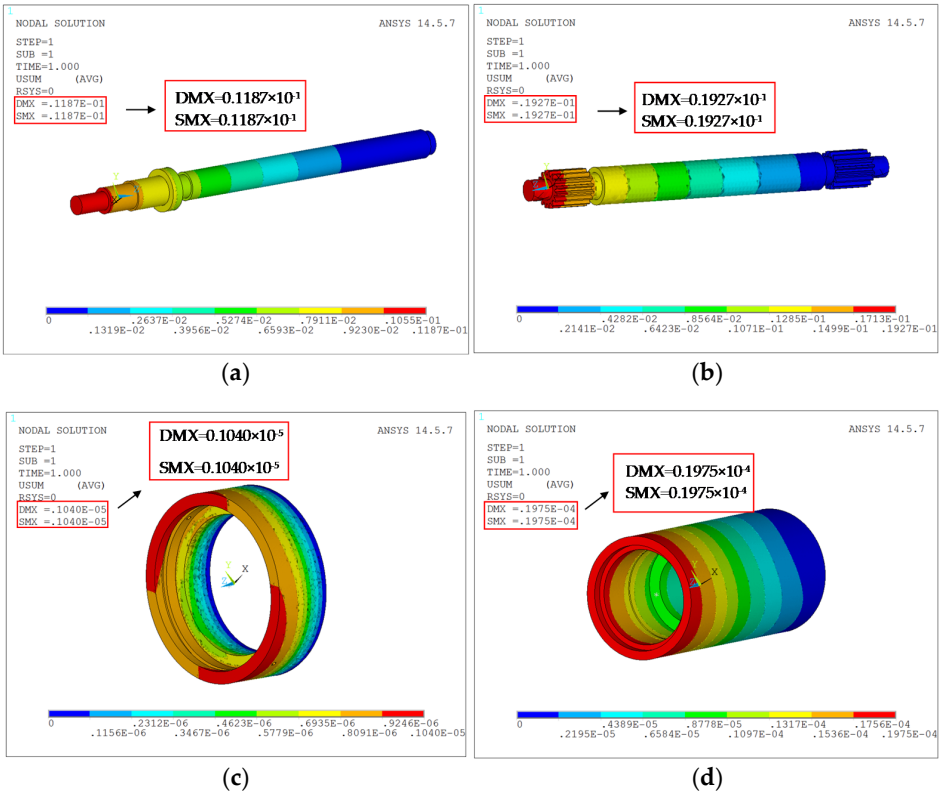

Figure 8. Bending deformation of component under radial load. (**a**) Bending deformation of the screw, (**b**) Bending deformation of the roller, (**c**) Bending deformation of the ring gear, (**d**) Bending deformation of the nut.

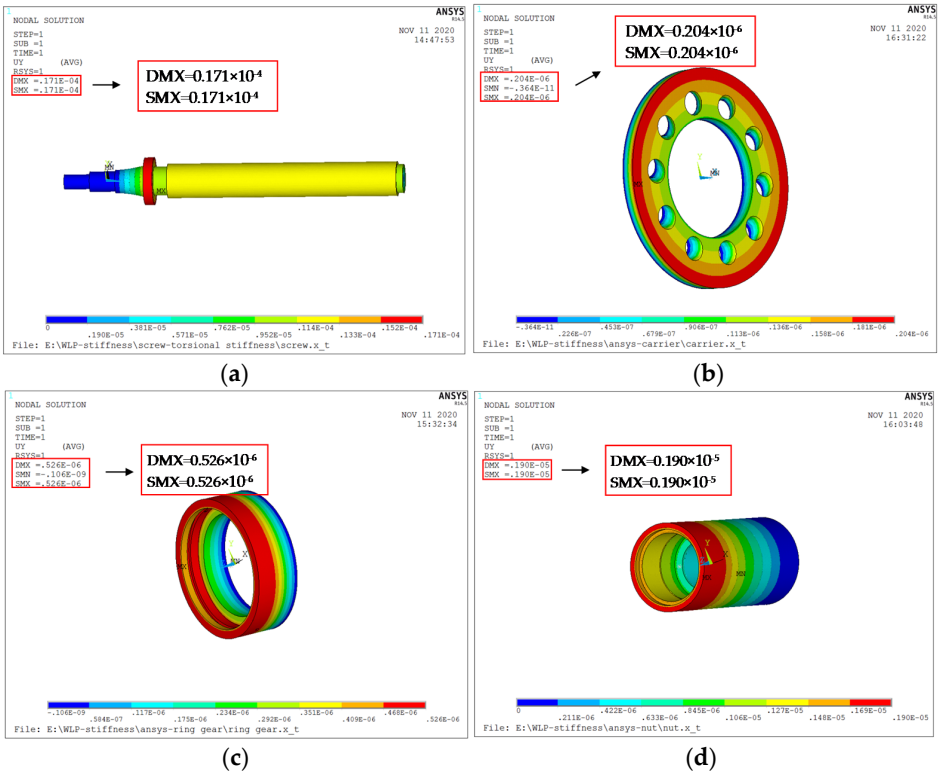

Figure 9. Torsional deformation of the component under torque. (**a**) Torsional deformation of the screw, (**b**) Torsional deformation of the carrier, (**c**) Torsional deformation of the ring gear, (**d**) Torsional deformation of the nut.

3. Natural Vibration Characteristics

In this paper, the influence of gyroscopic effect and friction force during thread meshing is ignored in the analysis of natural vibration characteristics. The structural parameters are shown in Table 3, and the calculation results of the mass and stiffness parameters of each component are shown in Table 4. Analyzing the natural vibration characteristics of the system can be transformed into solving the solution of undamped free vibration equations. The solution method is shown in Equation (55).

$$\omega_i^2 \cdot \boldsymbol{M} \cdot \boldsymbol{\varphi}_i = (\boldsymbol{K}_b + \boldsymbol{K}_m)\boldsymbol{\varphi}_i \tag{53}$$

$$\left(\boldsymbol{K}_b + \boldsymbol{K}_m - \omega_i^2 \boldsymbol{M}\right)\boldsymbol{\varphi}_i = 0 \tag{54}$$

$$\left|\boldsymbol{K}_b + \boldsymbol{K}_m - \omega_i^2 \boldsymbol{M}\right| = 0 \tag{55}$$

where ω_i is the i-th natural frequency; φ_i is the i-th eigenvector corresponding to the i-th vibration mode; $\boldsymbol{M}$ is the mass matrix, which can be expressed by Equation (21); $\boldsymbol{K}_b$ and $\boldsymbol{K}_m$ are the stiffness matrix, and the specific expression is shown in Equations (22)–(34).

Table 3. Structural parameters of PRSM.

Parameters \ Name	Units	Screw	Roller	Nut
Nominal diameters	mm	24	8	40
Major diameter	mm	24.65	8.8	39.26
Minor diameter	mm	22.5	6.95	41.05
Pitch	mm	2	2	2
Number of starts	—	5	1	1
Helical angle	°	7.55	4.55	4.55
Flank angle	°	45	45	45
Roller profile radius	mm	—	4.956	—
Gear				
Number of teeth	—	—	16	80
Tooth width	mm	—	10	10
Modulus	—	—	0.5	0.5
Modification coefficients	—	—	1	1
Dedendum	—	—	0.6	0.6
Pressure angle	°	—	20	20
Helical angle	°	—	0	0

Table 4. Stiffness parameters of PRSM.

Parameters	Units	Screw	Roller	Nut	Ring Gear	Carrier
Mass	kg	1.265	0.0326	2.159	0.112	0.023
Moment of inertia	kg·m^2	1.822×10^{-4}	5.216×10^{-7}	8.636×10^{-4}	4.48×10^{-5}	5.888×10^{-6}
Torsional stiffness	N·m/rad	6.241×10^{4}	—	9.359×10^{6}	3.380×10^{6}	6.983×10^{6}
Bending stiffness	N/m	3.571×10^{5}	2.199×10^{5}	2.228×10^{8}	4.160×10^{9}	—
Thread contact stiffness	N/m	2.078×10^{8}	—	2.198×10^{8}	—	—
Meshing stiffness	N/m	—	—	—	2.464×10^{8}	—

The bending-torsional coupling dynamic model proposed by the lumped mass method is universal for the system that can meet the assembly conditions of PRSM. According to the structural parameters provided in Table 3, when the number of rollers is 7, 8, 9, 10, 11 and 12, respectively, the natural frequencies can be obtained by means of looking for zeros of the characteristic determinant in Equation (55). Table 5 shows the number of natural frequencies and the order of natural frequency corresponding to different multiple roots when the number of rollers is different.

Table 5. Natural frequency of PRSM.

Number of Rollers (N)	Multiple Roots (m)			Number of Rollers (N)	Multiple Roots (m)		
	$m = 1$	$m = 2$	$m = N - 3$		$m = 1$	$m = 2$	$m = N - 3$
7	834	2995	14,801	10	708	3706	14,081
	4312	5712			5129	6977	
	5151	12,569			6131	11,584	
	18,047	28,406			18,648	27,525	
	22,308				26,055		
8	785	3248	14,081	11	677	3917	14,801
	4602	6148			5371	7380	
	5499	12,269			6421	11,215	
	18,268	28,104			18,815	27,248	
	23,637				27,169		
9	743	3485	14,801	12	650	4117	14,801
	4874	6567			5601	7780	
	5824	11,945			6697	10,808	
	18,466	27,811			18,971	26,979	
	24,881				28,233		

It can be seen from Table 5 that there is a certain mapping relationship between the natural frequency and the number of multiple roots [19]. When $m = 1$ and $m = 2$, the change of the number of rollers will not affect the number of natural frequencies, but only its value; when $m = N - 3$ ($N > 3$), the change of the number of rollers only affects the change of the number of natural frequencies, but it does not affect the value.

By solving the eigenvalue of Equation (53), the vibration modes of each order of PRSM with N rollers and meeting the assembly conditions can be obtained [33]. Taking the number of rollers $N = 7$ as an example, the natural frequency and vibration modes of PRSM based on bending-torsional coupling dynamic model are solved, as shown in Table 6. (1) Under the first natural frequency with $m = 1$, there is only torsional vibration of the carrier. Therefore, according to the characteristics of its vibration mode, it is defined as the carrier mode; under other natural frequencies with $m = 1$, the vibration modes of the screw, ring gear and nut are torsional vibrations, and there is no vibration in the x direction and y direction. The vibration modes of all rollers are torsional vibrations, and the modes are the same, and thus, it should be defined as the roller mode. (2) Among the four vibration modes corresponding to the natural frequency with $m = 2$, the screw, ring gear and nut appear transverse vibration in the x and y directions without torsional vibration. Each roller does complex torsional vibration, and the vibration state is different. These four vibration modes can be attributed to the transverse mode. (3) In the vibration mode corresponding to the natural frequency with $m = N - 3$ ($N > 3$), there is only torsional vibration of the roller, and therefore, it is known as the roller mode.

3.1. Carrier Mode

The characteristics of the mode shapes of the carrier mode are as follows:

(1) The multiple root $m = 1$;
(2) There is no torsional vibration and transverse vibration of the screw, ring gear and nut;
(3) The vibration state of each roller is the same: $\varphi_{Riu} = \varphi_{R1u} = 0$, $i = 1, 2, \ldots, N$.

Table 6. Vibration modes of PRSM with 7 rollers.

Natural Frequency (f)		**834 (m = 1)**	**4312**	**5151 (m = 1)**	**18,047**	**22,308**	**2995**	**5712 (m = 2)**	**12,569**	**28,406**	**14,081 ($m = N - 1$)**
Vibration modes	φ_{sx}	0	0	0	0	0	−0.45	−0.02	−0.02	−0.02	0
	φ_{sy}	0	0	0	0	0	−0.05	0.73	0.22	0.007	0
	φ_{su}	0	−0.85	0.17	−0.18	0.04	0	0	0	0	0
	φ_{rx}	0	0	0	0	0	0.02	0.21	−0.77	−1.08	0
	φ_{ry}	0	0	0	0	0	0.04	−0.10	0.43	−2.63	0
	φ_{ru}	0	−0.29	0.34	1.03	−2.77	0	0	0	0	0
	φ_{nx}	0	0	0	0	0	0.06	0.31	0.14	0.005	0
	φ_{ny}	0	0	0	0	0	0.58	−0.01	−0.011	−0.01	0
	φ_{nu}	0	−0.15	−0.66	0.10	−0.03	0	0	0	0	0
	φ_{R1u}	0	−0.31	0.32	1.88	0.77	−0.11	0.67	−2	−0.66	3.12
	φ_{R2u}	0	−0.31	0.32	1.88	0.77	0.04	0.91	−2.60	0.06	−3.33
	φ_{R3u}	0	−0.31	0.32	1.88	0.77	0.15	0.46	−1.24	0.73	−0.07
	φ_{R4u}	0	−0.31	0.32	1.88	0.77	0.15	−0.33	1.05	0.85	2.63
	φ_{R5u}	0	−0.31	0.32	1.88	0.77	0.04	−0.88	2.55	0.33	−1.34
	φ_{R6u}	0	−0.31	0.32	1.88	0.77	−0.11	−0.76	2.13	−0.44	−0.86
	φ_{R7u}	0	−0.31	0.32	1.88	0.77	−0.17	−0.07	0.10	−0.88	−0.15
	φ_{cu}	1.984	0	0	0	0	0	0	0	0	0

Assuming that the natural frequency is ω_i, the mode shapes of the carrier mode can be expressed by

$$\varphi_i = \varphi_{cu} \tag{56}$$

Equation (54) can be simplified based on Equation (56):

$$\left(K_{cu} - \omega_i^2 \cdot \frac{Jc + \sum_{i=1}^{N} m_{Ri} r_{c0}^2}{r_{c0}^2} \right) \varphi_{cu} = 0 \tag{57}$$

The natural frequency of the carrier mode can be written as

$$\omega_i = \sqrt{\frac{K_{cu} \cdot r_{c0}^2}{J_c + \sum_{i=1}^{N} m_{Ri} r_{c0}^2}} \tag{58}$$

From the analytic expression of natural frequency, it can be seen that the natural frequency of the carrier mode is related to the moment of inertia, nominal radius, torsional stiffness of the carrier and the mass of the roller. There is only one natural frequency corresponding to this vibration mode. It is found that the number of rollers N will not affect the number of natural frequencies but only the value of natural frequencies.

3.2. Torsional Mode

The mode shapes of the torsional mode have the following characteristics:

(1) The multiple root $m = 1$;
(2) The vibration state of each roller is the same: $\varphi_{Riu} = \varphi_{R1u} = 0$, $i = 1, 2, \ldots, N$;
(3) There is no transverse vibration of the screw, ring gear and nut;
(4) The amplitude of the carrier in the torsional direction is zero.

The mode shapes of the carrier mode can be expressed by:

$$\boldsymbol{\varphi}_i = [0, 0, \varphi_{su}, 0, 0, \varphi_{ru}, 0, 0, \varphi_{nu}, \varphi_{R1u}, \cdots, \varphi_{R1u}, 0]^{\mathrm{T}} \tag{59}$$

Since the vibration state of each roller is the same, Equation (54) can be described as

$$\left(\boldsymbol{K}^{'}{}_{b}+\boldsymbol{K}^{'}{}_{m}-\omega_i^2\boldsymbol{M}^{'}\right)\boldsymbol{\varphi}^{'}{}_{i}=0 \tag{60}$$

where

$$\boldsymbol{\varphi}^{'}{}_{i}=[\varphi_{su},\varphi_{ru},\varphi_{nu},\varphi_{R1u}]^{\mathrm{T}} \tag{61}$$

$$\boldsymbol{K}^{'}{}_{b}=diag[K_{su},K_{ru},K_{nu},0] \tag{62}$$

$$\boldsymbol{M}^{'}=diag\left[m_{eq,s},m_{eq,r},m_{eq,n},m_{eq,R1}\right] \tag{63}$$

$$\boldsymbol{K}^{'}{}_{m}=\begin{bmatrix} -k_{sR1}\cdot\cos^2_{\beta_R} & 0 & 0 & -k_{sR1}\cdot\cos^2_{\beta_R} \\ 0 & -k_{rR1} & 0 & k_{rR1} \\ 0 & 0 & -k_{nR1}\cdot\cos^2_{\beta_R} & k_{nR1}\cdot\cos^2_{\beta_R} \\ -k_{sR1}\cdot\cos^2_{\beta_R} & -k_{rR1} & -k_{nR1}\cdot\cos^2_{\beta_R} & -k_{sR1}\cdot\cos^2_{\beta_R}+k_{rR1}+k_{nR1}\cdot\cos^2_{\beta_R} \end{bmatrix} \tag{64}$$

The natural frequency and mode shapes under the torsional mode can be obtained quickly based on the simplified lower-order matrix. It can be seen from Equations (61)–(64) that there are four natural frequencies in the torsional mode, and the number of natural frequencies will not change with the number of rollers, but only the value will change. It is also found that the moment of inertia of the screw, ring gear, nut, carrier and roller will affect the natural frequency.

3.3. Transverse Mode

The mode characteristics of the transverse mode are as follows:

(1) The multiple root $m = 2$;
(2) There is a proportional relationship between the torsional mode shapes of each roller: $\varphi_{Riu} = \xi_i\varphi_{R1u}$, $i = 1, 2, \ldots, N$;
(3) The amplitude of the screw, ring gear, nut and carrier in the torsional direction is zero.

The mode shapes of the transverse mode can be expressed as

$$\boldsymbol{\varphi}_i=\left[\varphi_{sx},\varphi_{sy},0,\varphi_{rx},\varphi_{ry},0,\varphi_{nx},\varphi_{ny},0,\varphi_{R1u},\cdots,\xi_i\varphi_{R1u},0\right]^{\mathrm{T}} \tag{65}$$

$$\sum_{i=2}^{N}\xi_i+1=0 \tag{66}$$

Substituting Equations (65) and (66) into Equation (54) can obtain a simpler eight-dimensional matrix, and its formula is shown as

$$\left(\boldsymbol{K}^{''}{}_{b}+\boldsymbol{K}^{''}{}_{m}-\omega_i^2\boldsymbol{M}^{''}\right)\boldsymbol{\varphi}^{''}{}_{i}=0 \tag{67}$$

$$\boldsymbol{\varphi}^{''}{}_{i}=\left[\varphi_{sx},\varphi_{sy},\varphi_{rx},\varphi_{ry},\varphi_{nx},\varphi_{ny},\varphi_{R1u},\varphi_{R2u}\right]^{\mathrm{T}} \tag{68}$$

$$\boldsymbol{M}^{''}=diag\left[m_s,m_s,m_r,m_r,m_n,m_n,m_{eq,R1},m_{eq,R2}\right] \tag{69}$$

$$\boldsymbol{K}^{''}{}_{b}=diag\left[K_{sx},K_{sy},K_{rx},K_{ry},K_{nx},K_{ny},0,0\right] \tag{70}$$

$$\boldsymbol{K}^{''}{}_{m}=\begin{bmatrix} \boldsymbol{k}^{'}{}_{s} & \boldsymbol{k}^{'}{}_{0} & \boldsymbol{k}^{'}{}_{0} & \boldsymbol{k}^{'}{}_{s1,2} \\ & \boldsymbol{k}^{'}{}_{r} & \boldsymbol{k}^{'}{}_{0} & \boldsymbol{k}^{'}{}_{r1,2} \\ & & \boldsymbol{k}^{'}{}_{n} & \boldsymbol{k}^{'}{}_{n1,2} \\ & & & \boldsymbol{k}^{'}{}_{1,2} \end{bmatrix} \tag{71}$$

where

$$\boldsymbol{k}'_s = \boldsymbol{k}'_s(1) + \boldsymbol{k}'_s(2)$$
$$\begin{cases} \boldsymbol{k}'_s(1) = \begin{bmatrix} -K_{sR1}\sin^2\phi_{s1}\cos^2\beta_R & K_{sR1}\cos\phi_{s1}\sin\phi_{s1}\cos^2\beta_R \\ symmetric & -K_{sR1}\cos^2\phi_{s1}\cos^2\beta_R \end{bmatrix} \\ \boldsymbol{k}'_s(2) = \begin{bmatrix} -K_{sR2}\sin^2\phi_{s2}\cos^2\beta_R & K_{sR2}\cos\phi_{s2}\sin\phi_{s2}\cos^2\beta_R \\ symmetric & -K_{sR2}\cos^2\phi_{s2}\cos^2\beta_R \end{bmatrix} \end{cases} \tag{72}$$

$$\boldsymbol{k}'_r = \boldsymbol{k}'_r(1) + \boldsymbol{k}'_r(2)$$
$$\begin{cases} \boldsymbol{k}'_r(1) = \begin{bmatrix} -K_{rR1}\sin^2\phi_{r1} & K_{rR1}\cos\phi_{r1}\sin\phi_{r1} \\ symmetric & -K_{rR1}\cos^2\phi_{r1} \end{bmatrix} \\ \boldsymbol{k}'_r(2) = \begin{bmatrix} -K_{rR2}\sin^2\phi_{r2} & K_{rR2}\cos\phi_{r2}\sin\phi_{r2} \\ symmetric & -K_{rR2}\cos^2\phi_{r2} \end{bmatrix} \end{cases} \tag{73}$$

$$\boldsymbol{k}'_n = \boldsymbol{k}'_n(1) + \boldsymbol{k}'_n(2)$$
$$\begin{cases} \boldsymbol{k}'_n(1) = \begin{bmatrix} -K_{nR1}\sin^2\phi_{n1}\cos^2\beta_R & K_{nR1}\cos\phi_{n1}\sin\phi_{n1}\cos^2\beta_R \\ symmetric & -K_{nR1}\cos^2\phi_{n1}\cos^2\beta_R \end{bmatrix} \\ \boldsymbol{k}'_n(2) = \begin{bmatrix} -K_{nR2}\sin^2\phi_{n2}\cos^2\beta_R & K_{nR2}\cos\phi_{n2}\sin\phi_{n2}\cos^2\beta_R \\ symmetric & -K_{nR2}\cos^2\phi_{n2}\cos^2\beta_R \end{bmatrix} \end{cases} \tag{74}$$

$$\boldsymbol{k}'_{s1,2} = \begin{bmatrix} K_{sR1}\sin\phi_{s1}\cos^2\beta_R & K_{sR2}\sin\phi_{s2}\cos^2\beta_R \\ -K_{sR1}\cos\phi_{s1}\cos^2\beta_R & -K_{sR2}\cos\phi_{s2}\cos^2\beta_R \end{bmatrix} \tag{75}$$

$$\boldsymbol{k}'_{r1,2} = \begin{bmatrix} -K_{rR1}\sin\phi_{r1} & -K_{rR2}\sin\phi_{r2} \\ K_{rR1}\cos\phi_{r1} & K_{rR2}\cos\phi_{r2} \end{bmatrix} \tag{76}$$

$$\boldsymbol{k}'_{n1,2} = \begin{bmatrix} -K_{nR1}\sin\phi_{n1}\cos^2\beta_R & -K_{nR2}\sin\phi_{n2}\cos^2\beta_R \\ K_{nR1}\cos\phi_{n1}\cos^2\beta_R & K_{nR2}\cos\phi_{n2}\cos^2\beta_R \end{bmatrix} \tag{77}$$

$$\boldsymbol{k}'_{1,2} = \begin{bmatrix} -K_{sR1}\cos^2\beta_R + K_{rR1} + K_{nR1}\cos^2\beta_R & 0 \\ 0 & -K_{sR2}\cos^2\beta_R + K_{rR2} + K_{nR2}\cos^2\beta_R \end{bmatrix} \tag{78}$$

Matrix $\boldsymbol{k}'_0$ is a second-order matrix whose elements are all zero. Equations (68)–(71) show that the main factors affecting the natural frequency of the transverse mode, including the mass and bending stiffness of the screw, ring gear and nut, the contact stiffness of the thread, the meshing stiffness, along with the moment of inertia of the roller.

3.4. Roller Mode

The mode shape characteristics of the roller mode are as follows:

(1) The multiple root $m = N - 3$;
(2) There is no transverse vibration and torsional vibration of the screw, ring gear and nut: $\varphi_{sx} = \varphi_{sy} = \varphi_{su} = \varphi_{rx} = \varphi_{ry} = \varphi_{ru} = \varphi_{nx} = \varphi_{ny} = \varphi_{nu} = 0$;
(3) The amplitude of the carrier in the torsional direction is zero: $\varphi_{cu} = 0$.
(4) The relationship between the mode shapes of each roller can be expressed as

$$\varphi_{Riu} = \xi_i \varphi_{R1u} \tag{79}$$

$$\sum_{i=2}^{N} \xi_i = 0 \tag{80}$$

The mode shapes of the roller mode can be described as

$$\boldsymbol{\varphi}_i = [0, 0, 0, 0, 0, 0, 0, 0, 0, \varphi_{R1u}, \cdots, \xi_i \varphi_{R1u}, 0]^{\mathrm{T}} \tag{81}$$

Similarly, the sub eigenvalues corresponding to the roller mode can be obtained through combining Equations (54) and (79)–(81):

$$\left(\boldsymbol{K}^{'''}{}_{b}+\boldsymbol{K}^{'''}{}_{m}-\omega_i^2\boldsymbol{M}^{'''}\right)\boldsymbol{\varphi}^{'''}{}_{i}=0 \tag{82}$$

where

$$\boldsymbol{\varphi}^{'''}{}_{i}=[\varphi_{R1u},\cdots,\xi_i\varphi_{R1u}]^{\mathrm{T}} \tag{83}$$

$$\boldsymbol{M}^{'''}=diag\left[m_{eq,R1},\cdots,m_{eq,Ri}\right] \tag{84}$$

$$\boldsymbol{K}^{'''}{}_{b}=diag[0,\cdots,0] \tag{85}$$

$$\boldsymbol{K}^{'''}{}_{m}=diag\left[\begin{array}{ccc}\boldsymbol{K}^{'''}{}_{m}(1) & \boldsymbol{K}^{'''}{}_{m}(2) & \boldsymbol{K}^{'''}{}_{m}(3)\end{array}\right] \tag{86}$$

$$\begin{cases}\boldsymbol{K}^{'''}{}_{m}(1)=diag\left[-K_{sR1}\cdot\cos^2\beta_R,\cdots,-K_{sRi}\cdot\cos^2\beta_R\right]\\ \boldsymbol{K}^{'''}{}_{m}(2)=diag[K_{rR1},\cdots,K_{rRi}]\\ \boldsymbol{K}^{'''}{}_{m}(3)=diag\left[K_{nR1}\cos^2\beta_R,\cdots,K_{nRi}\cos^2\beta_R\right]\end{cases} \tag{87}$$

Equation (82) is simplified by substituting the specific parameter of each matrix through Equations (83)–(87):

$$\left(\begin{array}{c}-K_{sRi}\cdot\cos^2\beta_R+K_{rRi}\\ +K_{nRi}\cdot\cos^2\beta_R-\omega_i^2\cdot\frac{J_{Ri}}{r_{Ri}^2}\end{array}\right)\cdot\xi_i\varphi_{R1u}=0 \tag{88}$$

The analytic expression of the natural frequency in the roller mode can be deduced:

$$\omega_i=\sqrt{\frac{(-K_{sRi}\cdot\cos^2\beta_R+K_{rRi}+K_{nRi}\cdot\cos^2\beta_R)r_{Ri}^2}{J_{Ri}}} \tag{89}$$

It is apparent from the analytic expression that the natural frequency of the roller mode is related to the moment of inertia, helical angle, the contact stiffness and meshing stiffness of the roller, but it is independent of the torsional stiffness and the number of rollers. When the multiple root $m = N - 3$, the number of rollers does not have an effect on the value of natural frequency but only the number of natural frequencies from Table 4, which is consistent with the result of the analytical expression of natural frequency.

4. Verification

The influence for the change of roller radius on the thread contact stiffness is displayed in Figure 10, where (a) is the effect of the roller radius on the thread contact stiffness under the structural parameters of PRSM, as shown in Table 3; (b) is the law of influence under the condition of Ref. [24]. It can be seen that the influence law of the roller radius on the thread contact stiffness calculated by the model in this paper is in good agreement with the law obtained from Ref. [24]. With the increase in roller radius, the thread contact stiffness is also increasing, but the speed is gradually slower; under different contact angles, when the roller radius increases to a certain range, it is almost impossible to change the contact stiffness by changing the value of the roller radius. The value difference between the two models is mainly due to the fact that the number of threads and design details of the screw, roller and nut are not described in detail; consequently, this paper only compares the trend phenomenon with the conclusion in Ref. [24]. The reason why the roller radius affects the contact stiffness is that the selection of the roller radius is related to the design of the roller thread profile [34]. When the roller radius is increased, the thread contact curvature radius will increase synchronously, which further affects the improvement of contact stiffness. According to the structural design principle of PRSM, the structural parameters of the screw, roller and nut are closely related. The radius of the screw and nut will increase with the growth of the roller radius, which will not only increase the thread

contact radius but also improve body stiffness of the component and the overall stiffness of PRSM.

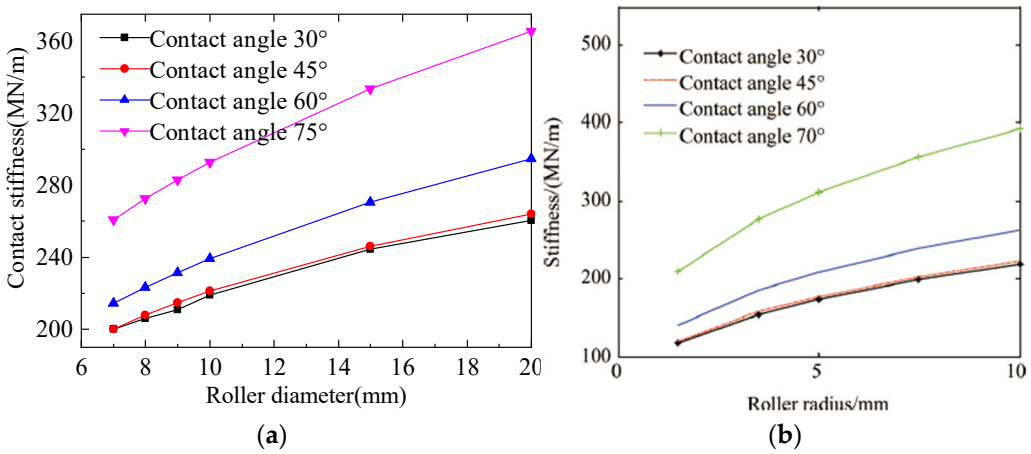

Figure 10. The influence of roller radius on contact stiffness. (**a**) Model in this paper (**b**) Model in Ref. [24].

As shown in Figure 11a,b, the law for the change of contact angle on the contact stiffness is displayed based on the model in this paper and in Ref. [24], respectively. It is shown that when the rollers take different radii, the contact stiffness is enhanced with the increase in thread contact angle, and the growth rate increases.

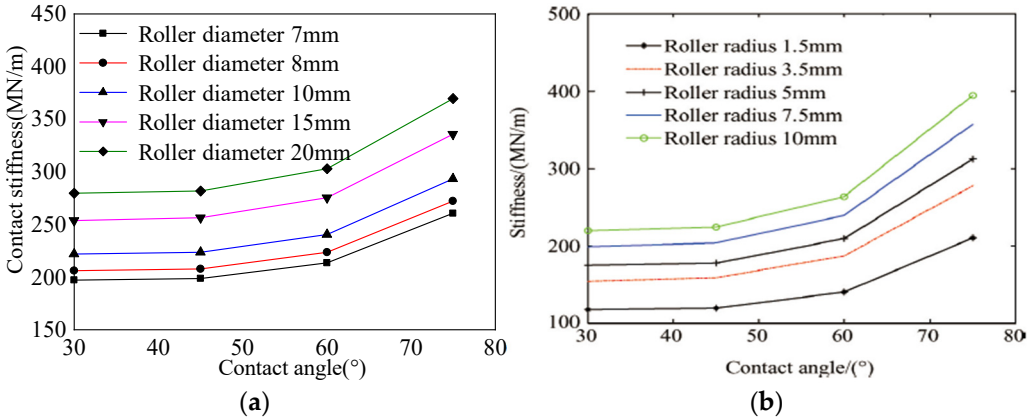

Figure 11. The influence of contact angle on contact stiffness. (**a**) Model in this paper (**b**) Model in Ref. [24].

According to the formula of contact stiffness, the contact angle is related to the contact stiffness, and the natural frequency of the system will be affected by contact stiffness. Further, the change of the contact angle will have an effect on its natural frequency. When the nominal diameter of the roller is 8 mm, the influence trend of the change of thread contact angle on the first-order natural frequency is obtained. As shown in Figure 12a, the first natural frequency increases monotonically with the contact angle increasing. The dynamic model of PRSM in Ref. [24] was established according to the finite element method. On this basis, when the nominal diameter of the roller is 7 mm, the influence of the contact angle on the first-order natural frequency is shown in Figure 12b. It is also indicated that when the contact angle increases, the first-order natural frequency under the two dynamic models shows a monotonic increasing trend, and its change rate gradually accelerates. In general, the purpose of changing the first-order natural frequency of PRSM can be achieved by reasonably changing the contact angle. The reason why the natural frequency value shown in Figure 12a is significantly higher than that in Figure 12b is that the nominal

diameter of the roller thread selected in this paper is larger than that in Ref. [24]. In addition, the nominal diameter of the roller has a great influence on the first-order natural frequency, which is consistent with the law under the roller mode.

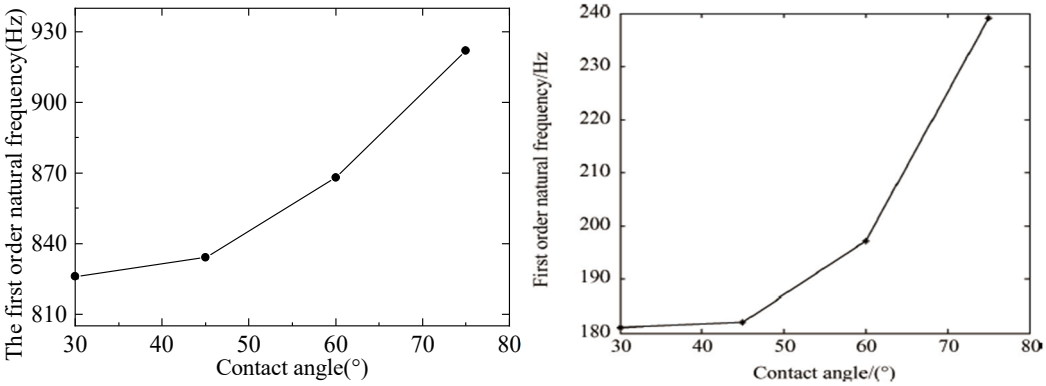

Figure 12. Influence of contact angle on the first natural frequency. (**a**) Model in this paper (**b**) Model in Ref. [24].

5. Conclusions

(1) This paper proposed a bending-torsional coupling dynamic model for the dynamic characteristics PRSM based on the lumped mass method. The lumped mass of the screw, ring gear, nut and roller, thread contact stiffness and meshing stiffness were taken into account. In addition, the torsional vibration of the roller and the transverse vibration of the screw, ring gear and nut became another key consideration.

(2) Based on the analysis of the contact point positions on the roller–screw side and roller–nut side, the analysis method of the vibration displacement between the two meshing parts of the PRSM was proposed. The projection and derivation progress of the relative displacement between the screw and the roller, the roller and the nut, as well as the roller and the ring gear, were mainly discussed. On this basis, the dynamic differential equations of the screw, ring gear, nut, roller and carrier were derived to form the multi degree of freedom differential equations of the PRSM. The calculation methods of mass parameters, thread contact stiffness and meshing stiffness were also discussed in detail.

(3) The natural vibration characteristics of the PRSM were studied according to the bending-torsional coupling dynamical model proposed in this paper. With that, four vibration modes and the main parameters affecting the vibration modes were summarized. Then, the analytic expressions of natural frequency under the carrier mode and the roller mode were deduced. The correctness of the bending-torsional coupling model was verified from three aspects, which has great directive meaning for further development of the structural design, vibration characteristics and dynamic response of the PRSM.

Author Contributions: Conceptualization, L.W.; methodology, L.W. and S.M.; software, L.W. and Q.H.; validation, P.D., Q.H. and L.W.; investigation, Q.H.; data curation, P.D. and S.M.; writing—original draft preparation, L.W.; writing—review and editing, L.W. and S.M.; visualization, L.W.; supervision, P.D. and S.M.; funding acquisition, S.M. All authors have read and agreed to the published version of the manuscript.

Funding: The research is supported by National Natural Science Foundation of China (Grant No. 51875458, 51905428), The Fundamental Research Funds for the Central Universities (Grant No. 31020200506004), National Key R&D Program of China (Grant No. 2019YFB2004700), and Key R&D Projects in Shaanxi Province (Grant No. 2021ZDLGY10-08).

Conflicts of Interest: The authors declare no conflict of interest.

References

1. Cornelius, C.C.; Lawlor, S.P. Roller Screw System. U.S. Patent 7,044,017 (B2), 16 May 2006.
2. Jin, Q.Z.; Yang, J.J.; Sun, L. The comparative research on the static stiffness of ball screw and planetery roller screw. *Mech. Sci. Technol.* **1999**, *18*, 230–232. (In Chinese)
3. Brandenburg, G.; Bruckl, S.; Dormann, J. Comparative investigation of rotary and linear motor feed drive systems for high precision machine tools. In Proceedings of the 6th International Workshop on Advanced Motion Control, Nagoya, Japan, 30 March–1 April 2002; pp. 384–389. [CrossRef]
4. Falkner, M.; Nitschko, T.; Supper, L.; Traxler, G.; Zemann, J.V.; Roberts, E.W. Roller screw lifetime under oscillatory motion: From dry to liquid lubrication. In Proceedings of the 10th European Space Mechanisms and Tribology Symposium, San Sebastian, Spain, 24–26 September 2003.
5. Ohashi, Y.; De, A.A.; Nose, Y. Hemolysis in an electromechanical driven pulsatile total artificial heart. *Artif. Organs* **2003**, *27*, 1089–1093. [CrossRef] [PubMed]
6. Nosov, A.S. Power electromechanical drive based on planetary roller-screw gear of improved accuracy. *Vestn. Mosk. Aerosp. MAI J.* **2015**, *22*, 100–107.
7. Li, J.M.; Yu, Z.Y.; Huang, Y.P.; Li, Z. A review of electromechanical actuation system for more electric aircraft. In Proceedings of the IEEE/CSAA International Conference on Aircraft Utility Systems, Beijing, China, 10–12 October 2016.
8. Liu, Y.Q.; Wang, J.S.; Cheng, H.G.; Sun, Y. Kinematics analysis of the roller screw based on the accuracy of meshing point calculation. *Math. Probl. Eng.* **2015**, *5*, 303972. [CrossRef]
9. Liu, Y.Q.; Shang, Y.; Wang, J.S. Mathematical analysis of the meshing performance of planetary roller screws applying different roller thread shapes. *Adv. Mech. Eng.* **2017**, *9*, 361–364. [CrossRef]
10. Ma, S.; Wu, L.; Liu, G.; Fu, X. Optimal design and contact analysis for planetary roller screw. *Appl. Mech. Mater.* **2011**, *86*, 361–364. [CrossRef]
11. Ma, S.; Wu, L.; Liu, G.; Fu, X. Local contact characteristics of threaded surfaces in a planetary roller screw mechanism. *Mech. Based Des. Struct. Mach.* **2019**, *139*, 212–236. [CrossRef]
12. Ma, S.; Wu, L.; Fu, X.; Li, Y.; Liu, G. Modelling of static contact with friction of threaded surfaces in a planetary roller screw mechanism. *Mech. Mach. Theory* **2019**, *139*, 212–236. [CrossRef]
13. Hojjat, M.Y.; Mahdi, A. A comprehensive study on capabilities and limitations of roller-screw with emphasis on slip tendency. *Mech. Mach. Theory* **2009**, *44*, 1887–1899. [CrossRef]
14. Jones, M.H.; Velinsky, S.A. Contact kinematics in the roller screw mechanism. *J. Mech. Des.* **2013**, *135*, 051003. [CrossRef]
15. Jones, M.H.; Velinsky, S.A. Stiffness of the roller screw mechanism by the direct method. *Mech. Based Des. Struct. Mach.* **2014**, *42*, 17–34. [CrossRef]
16. Sandu, S.; Biboulet, N.; Nelias, D.; Abevi, F. An efficient method for analyzing the roller screw thread geometry. *Mech. Mach. Theory* **2018**, *126*, 243–264. [CrossRef]
17. Sandu, S.; Biboulet, N.; Nelias, D.; Abevi, F. Analytical prediction of the geometry of contact ellipses and kinematics in a roller screw versus experimental results. *Mech. Mach. Theory* **2019**, *131*, 115–136. [CrossRef]
18. Vahid, O.; Eslaminasab, N.; Golnaraghi, M.F. Friction-induced vibration in lead screw systems: Mathematical modeling and experimental studies. *J. Vib. Acoust.* **2009**, *131*, 021003. [CrossRef]
19. Jones, M.H.; Velinsky, S.A. Kinematics of roller migration in the planetary roller screw mechanism. *J. Mech. Des.* **2012**, *134*, 061006. [CrossRef]
20. Jones, M.H.; Velinsky, S.A.; Lasky, T.A. Dynamics of the planetary roller screw mechanism. *J. Mech. Robot.* **2016**, *8*, 014503. [CrossRef]
21. Abevi, F.; Daidie, A.; Chaussumier, M.; Sartor, M. Static load distribution and axial stiffness in a planetary roller screw mechanism. *J. Mech. Des.* **2015**, *138*, 012301. [CrossRef]
22. Abevi, F.; Daidie, A.; Chaussumier, M.; Orieux, S. Static analysis of an inverted planetary roller screw mechanism. *J. Mech. Robot.* **2016**, *8*, 041020. [CrossRef]
23. Ma, S.; Zhang, T.; Liu, G.; He, J. Bond Graph-based dynamic model of planetary roller screw mechanism with consideration of axial clearance and friction. *Proc. Inst. Mech. Eng. Part C J. Mech. Eng. Sci.* **2018**, *232*, 2899–2911. [CrossRef]
24. Guo, J.N.; He, P.; Huang, H.Y. Theoretical investigation and experimental study on planetary roller screw dynamics. *J. Propuls. Technol.* **2018**, *39*, 841–848. (In Chinese)
25. Wu, L.P.; Ma, S.J.; Wan, Q.; Liu, G. Dynamic modal of planetary roller screw mechanism with considering torsional degree of freedom. In Proceedings of the 6th International Conference on Mechatronics and Mechanical Engineering, Osaka, Japan, 27–30 September 2019.
26. Fu, X.; Liu, G.; Tong, R.; Ma, S.; Lim, T.C. A nonlinear six degrees of freedom dynamic model of planetary roller screw mechanism. *Mech. Mach. Theory* **2018**, *119*, 22–36. [CrossRef]
27. Fu, X.; Liu, G.; Ma, S.; Tong, R.; Li, X. An efficient method for the dynamic analysis of planetary roller screw mechanism. *Mech. Mach. Theory* **2020**, *150*, 103851. [CrossRef]
28. Du, X.; Chen, B.; Zheng, Z. Investigation on mechanical behavior of planetary roller screw mechanism with the effects of external loads and machining errors. *Tribol. Int.* **2021**, *154*, 106689. [CrossRef]

29. Lepagneul, J.; Tadrist, L.; Sprauel, J.-M.; Linares, J.-M. Fatigue lifespan of a planetary roller-screw mechanism. *Mech. Mach. Theory* **2022**, *172*, 104769. [CrossRef]
30. Johnson, K.L. *Contact Mechanics*; Cambridge University Press: Cambridge, UK, 1985; pp. 84–104.
31. Tian, Y.T.; Li, G.X.; Tong, W.; Wu, C.H. A finite element based study of the load distribution of a heavily loaded spur gear system with effects of transmission shafts and gear blanks. *J. Sound Vib.* **2003**, *125*, 625–631.
32. National Gear Standardization Technical Committee. *Compilation of Parts and Related Standards: Gear and Gear Transmission*; Standards Press of China: Beijing, China, 2012; Volume 1, pp. 158–187. (In Chinese)
33. Song, Y.M.; Zhang, J. Inherent characteristics of 3K-ii spur planetary gear trains. *J. Mech. Eng.* **2009**, *45*, 23–28. (In Chinese) [CrossRef]
34. Yang, J.J.; Wei, Z.X.; Zhu, J.S.; Wei, D. Calculation of load distribution of planetary roller screw and static rigidity. *J. Huazhong Univ. Sci. Technol. (Nat. Sci. Ed.)* **2011**, *39*, 1–4. (In Chinese)